AIAA JOURNAL
Vol. 49, No. 10, October 2011

Investigation of a High-Mach-Number Overexpanded Jet Using Large-Eddy Simulation

Nicolas de Cacqueray,* Christophe Bogey,† and Christophe Bailly‡
École Centrale de Lyon, 69134 Ecully, France

DOI: 10.2514/1.J050952

An initially laminar overexpanded round jet at an exit Mach number of 3.30 and a Reynolds number of 10^5 is calculated by compressible large-eddy simulation. The near field obtained by large-eddy simulation is also propagated to the acoustic far field by solving the full Euler equations to take into account the nonlinear propagation effects. Both computations are performed using low-dissipation finite differences in combination with an adaptive shock-capturing method. The jet originates from a straight pipe nozzle of radius r_e, including lips of thickness $0.05r_e$. At the pipe exit, Blasius mean flow profiles are imposed, and static pressure and temperature are equal to 0.5×10^5 Pa and 360 K, resulting in fully adapted and acoustic Mach numbers, respectively, of 2.83 and 3.47. The jet flowfields, as well as the acoustic near and far fields, are described in detail and compared with data of the literature. The turbulent mechanisms developing in the jet are investigated, using spectral and azimuthal decompositions of the velocity fluctuations along the shear layers. Same analyses are applied to the acoustic fields, in order to discuss the properties of jet noise components. In this way, Mach waves, shock-associated noise, screech tones, and turbulent mixing noise are identified.

Nomenclature

a_n^θ	=	relative contribution of azimuthal modes n
c	=	local sound speed
c_∞	=	ambient field sound speed
f	=	frequency
f_c	=	cutoff frequency
f_{shock}	=	central frequency of the broadband shock-associated noise
f_{up}	=	frequency of the upstream-propagating shock-associated noise
L_{VS}	=	first shock length from vortex sheet, $2\pi(M_j^2-1)^{1/2}r_j/\mu_1$, $\mu_1 = 2.40483$
L_1	=	first shock length measured on the jet axis
M_a	=	acoustic Mach number
M_c	=	convection Mach number
M_e	=	exit Mach number
M_j	=	equivalent fully expanded exit Mach number, u_j/c_∞
n	=	azimuthal mode
p_e	=	exit static pressure
p_j	=	equivalent fully expanded exit static pressure
p'	=	fluctuating static pressure
$\langle p \rangle$	=	mean static pressure
Re	=	Reynolds number based on exit conditions
r_e	=	nozzle radius
r_j	=	equivalent fully expanded nozzle radius
St_c	=	cutoff Strouhal number
St_e	=	Strouhal number based on exit conditions
St_{up}	=	Strouhal number of the upstream-propagating shock-associated noise
T_e	=	exit temperature
u_{axis}	=	centerline mean axial velocity
u_c	=	convection velocity
u_e	=	exit velocity
u_j	=	equivalent fully expanded exit velocity
$\langle u_z \rangle$	=	mean axial velocity
$\langle u_z'^2 \rangle$	=	mean-square axial velocity fluctuations
$\langle u_z'^2 \rangle_n$	=	mean-square axial velocity fluctuations due to mode n
$\lvert\hat{u}_z^2\rvert(St_e, n)$	=	two-dimensional power spectral densities
z_1	=	first shock location on the jet axis
γ	=	specific heat ratio
Δr	=	mesh size in the radial direction
Δz	=	mesh size in the axial direction
δ	=	boundary-layer thickness in the pipe nozzle
$\delta_{0.5}$	=	jet half-width
μ_e	=	exit molecular viscosity
ρ_e	=	exit density
ϕ	=	radiation angle measured according to the flow direction

Presented as Paper 2010-3732 at the 16th AIAA/CEAS Aeroacoustics Conference, Stockholm, Sweden, 7 June–9 September 2010; received 22 September 2010; revision received 22 April 2011; accepted for publication 23 April 2011.

*Ph.D., Laboratoire de Mécanique des Fluides et d'Acoustique, UMR CNRS 5509; nicolas.decacqueray@gmail.com.

†CNRS Research Scientist, Laboratoire de Mécanique des Fluides et d'Acoustique, UMR CNRS 5509; christophe.bogey@ec-lyon.fr. Senior Member AIAA.

‡Professor, Laboratoire de Mécanique des Fluides et d'Acoustique, UMR CNRS 5509, and Institut Universitaire de France, 103 Boulevard Saint-Michel, 75005 Paris, France; christophe.bailly@ec-lyon.fr. Senior Member AIAA.

I. Introduction

PROPULSIVE jets generated by booster rockets of space launchers are characterized by high stagnation pressure and temperature, resulting [1] in fully expanded exit Mach numbers M_j usually around 3, and acoustic Mach numbers $M_a > M_j$. Such jets are known to radiate strong acoustic fields, which are assumed to be dominated by Mach waves [2–6]. Few aerodynamic and acoustic data are unfortunately available [1,7–10], and noise sources are still to be fully described [11].

In high-Reynolds-number subsonic jets, two noise components have been identified [12–15]. One dominates in the downstream direction with a noise source located around the end of the potential core [16,17], and another dominates in the sideline direction and is probably linked to the turbulent mixing in the shear layer [13,17]. The continuity of the acoustic spectra between subsonic and supersonic jets has been shown by Tam et al. [12], who suggested that the same noise components can be found in both cases. Specific noise components such as Mach waves and shock-associated noise are, however, generated in supersonic jets. Mach waves are radiated when

the convection velocity of turbulent structures is supersonic [18]. They are highly directive and have a conical wavelike geometry in the acoustic field. Other sound sources appear when a shock-cell structure is present in the jet plume generated by the adjustment of static pressure to the ambient field at the nozzle exit. The interactions between turbulent structures and shock cells result in broadband noise [19,20] propagating both in the upstream and downstream directions [19,21]. If the jet shear layer at the nozzle exit is sufficiently receptive to the upstream-propagating acoustic waves [22–24], a feedback loop can also be established. This loop generates a tonal noise called *screech* [25], whose fundamental frequency was shown to collapse with the central frequency of the broadband shock-associated noise in the upstream direction [23]. Note, finally, that in this case the whole jet oscillates at the fundamental and harmonic screech frequencies [22,26,27].

The noise components mentioned previously have been studied extensively for cold jets with fully expanded Mach numbers $M_j \leq 2$ and in a few works [1,3,7–10] for hot jets with $M_j \simeq 3$. Their contributions to heated, rocketlike jet noise, however, have not been well established, even if Mach waves radiated by linear instability waves [4,19] are usually assumed to be dominant [3,4]. They have, moreover, been found experimentally to vary strongly with the jet velocity and temperature. Regarding the effects of the temperature in particular, they may be significant on turbulent mixing noise [28], Mach waves [29], broadband shock-associated noise [30], and screech tones [19,31,32].

Further investigations of jet noise components can now be carried out directly by solving the Navier–Stokes equations [17,33,34], especially using large-eddy simulation (LES) for flows at high-Reynolds numbers [35]. Such simulations have, for instance, been performed by Bogey et al. [15,36,37] in order to study the influence of the Reynolds number and of the initial conditions in subsonic jets, by Viswanathan et al. [38] and Liu et al. [39] to improve the prediction of broadband shock-associated noise and screech tone for real nozzle geometries, and by Berland et al. [22] to investigate screech tone generation in a plane supersonic jet. In these works, the use of low-dissipation and low-dispersion numerical schemes is usually recommended [40–42] to ensure numerical accuracy. An appropriate shock-capturing method is also required specifically in supersonic flows to remove Gibbs oscillations near shocks [43,44]. In this case, particular attention must be paid to the possible spurious dissipation of the turbulent structures and the acoustic waves by the shock-capturing procedure [45].

In the present study, the noise radiated by an overexpanded heated jet at an exit Mach number of 3.30 is computed directly by a compressible LES using low-dissipation finite difference schemes [42,46] in combination with an adaptive shock-capturing procedure [44]. The jet exit parameters are chosen to be similar to those of an experiment of Varnier and Gély [9] providing near-field acoustic levels. Because of LES limitations, the Reynolds number of the computed jet is set to a value of 10^5, which is one order of magnitude lower than in the experiment, and the jet is initially laminar. The objective here is to obtain information on noise generation mechanisms in a supersonic jet at an exit Mach number of 3.30 with exit static pressure and temperature of 0.5×10^5 Pa and 360 K. With this aim in view, the jet flowfield is described in detail, in particular using spectral and azimuthal decompositions of the axial velocity fluctuations along the shear layer. The noise emitted by the jet is characterized in the near field from the LES data, as well as in the far field from solutions evaluated from the near field by solving the full Euler equations. Pressure levels and spectra are presented, and the azimuthal mode distributions of the sound fields are exhibited. Noise generation mechanisms are finally discussed, based on the connections between the turbulent flow and the acoustic field and on the sound source models available in the literature [23,47].

The outline of the paper is as follows. In Sec. II, the simulation parameters and the numerical procedure are presented. In Sec. III, snapshots of vorticity, numerical schlieren pictures, and fluctuating pressure are shown. In Sec. IV, the mean aerodynamic field is examined, and the properties of shear-layer velocity fluctuations are explored according to their azimuthal components. Near- and far-field acoustic results are presented in Sec. V, in which links between the turbulent flow and the acoustic fields are also displayed to identify the different noise components. Concluding remarks are provided in Sec. VI. The paper also contains an Appendix dealing with the importance of nonlinear effects in the far-field wave extrapolation.

II. Numerical Procedure

A. Simulation Parameters

An overexpanded jet at an exit Mach number of $M_e = 3.30$, an exit temperature of $T_e = 360$ K, and an exit static pressure of $p_e = 0.5 \times 10^5$ Pa, originating at $z = 0$ from a pipe nozzle of radius r_e, is computed. The stagnation pressure and temperature are 28.6×10^5 Pa and 1144 K. The specific heat ratio γ is constant in the present computation and equal to 1.4, and the resulting exit velocity is $u_e = 1255\ \mathrm{m \cdot s^{-1}}$. The equivalent fully expanded exit conditions defined from the same stagnation conditions and a static pressure of $p_j = 10^5$ Pa are a Mach number of 2.83, a temperature of 439 K, and a radius of $r_j = 0.81 r_e$. The acoustic Mach number M_a, defined as the ratio of the fully expanded velocity $u_j = 1190\ \mathrm{m \cdot s^{-1}}$ over the ambient sound speed $c_\infty = 343\ \mathrm{m \cdot s^{-1}}$, is 3.47. The Reynolds number estimated from the exit quantities is equal to $2 r_e u_e \rho_e / \mu_e = 0.94 \times 10^5$, where ρ_e and μ_e are the jet exit density and molecular viscosity. A straight pipe nozzle of length $0.5 r_e$ with $0.05 r_e$ wide lip is included in the computational domain to specify the inflow conditions. Therefore, the effects associated with the nozzle geometry [39] on the jet flow development as well as on the noise radiation mechanisms are not considered here. Inside the pipe, a Blasius profile for a laminar boundary layer of thickness $\delta = 0.05 r_e$ is imposed for the mean velocity, and a Crocco–Busemann profile is used for the mean density. Random pressure disturbances of low amplitude are introduced in the nozzle, yielding nozzle-exit maximum velocity fluctuations of 1% of the jet exit velocity.

The jet exit quantities M_e, p_e, and T_e are chosen to be very similar to those of an experiment conducted by Varnier and Gély using the MARTEL experimental facility [9] at Poitiers, as shown in Table 1. Owing to computational and LES limitations, the Reynolds number of the simulation is, however, smaller than the Reynolds number of the experiment.

B. Numerical Methods

The simulation is performed by solving the unsteady compressible Navier–Stokes equations in cylindrical coordinates, using low-dispersion and low-dissipation finite difference schemes [42,44,46]: explicit 11-point fourth-order finite differences and sixth-order filter for space discretization and a second-order six-stage Runge–Kutta algorithm for time integration. For the treatment of the axis singularity, the method proposed by Mohseni and Colonius [48] is used, and to increase the time step the effective azimuthal resolution is reduced near the jet centerline [49]. The LES approach is based on the explicit application of a relaxation filtering to the flow variables [50] to take into account the dissipative effects of the subgrid scales. Nonreflective acoustic boundary conditions [51] are implemented at the radial and upstream boundaries, and a sponge zone is used in the downstream direction to minimize acoustic reflections at the outflow boundary [51]. These numerical methods have been successfully implemented in LES of subsonic round jets [17,37,52] and of a supersonic screeching plane jet [22]. An adaptive and conservative shock-capturing method is in addition used to remove Gibbs oscillations near shocks [44].

Table 1 Jet exit parameters in the present computation and in the experiment of Varnier and Gély [9]: Mach number M_e, static pressure p_e, temperature T_e, and Reynolds number Re

Study	M_e	p_e	T_e	Re
Present computation	3.30	0.50×10^5 Pa	360 K	0.94×10^5
Varnier and Gély [9]	3.27	0.51×10^5 Pa	359 K	17.5×10^5

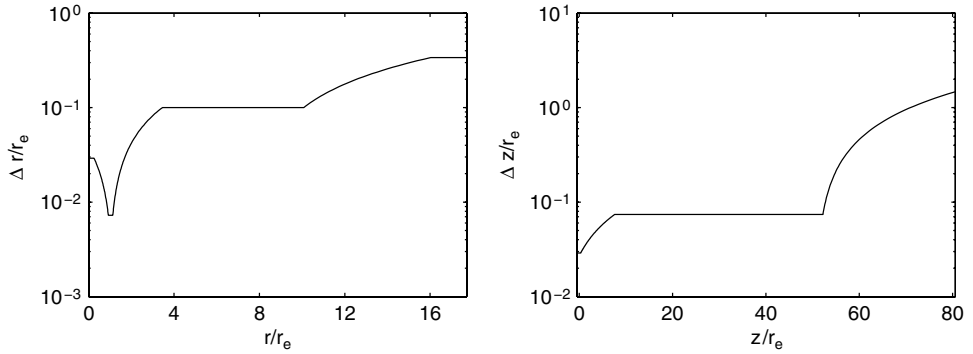

Fig. 1 Grid mesh sizes in the LES computation: a) radial mesh size Δr and b) axial mesh size Δz.

The grid used for the present jet contains $n_r \times n_\theta \times n_z = 256 \times 128 \times 840 = 28 \times 10^6$ points, and 120,000 iterations carried out using NEC SX-8 computers have been necessary to ensure statistical convergence. The radial and the axial mesh spacings are presented in Fig. 1. In the radial direction, the mesh size is $\Delta r = 0.0072 r_e$ at $r = r_e$, yielding seven points in the boundary layer as done previously for initially fully laminar subsonic jets [37]. It is stretched to obtain $\Delta r = 0.1 r_e$ at $r = 3.5 r_e$. Near the radial boundaries, the mesh size still increases in order to specify radiation boundary conditions at $r = 16.5 r_e$. In the axial direction, the mesh size is constant in the pipe nozzle, and it is equal to $\Delta z = 0.029 r_e$. Then, the mesh is stretched to reach $\Delta z = 0.074 r_e$ at $z = 7.5 r_e$. Finally, the sponge zone is built by increasing the axial mesh size from $z = 52 r_e$.

The LES data are recorded on two surfaces. The first one is located at $z = 0$, from $r = 1.15 r_e$ to $9.5 r_e$, and the second one is at $r = 9.5 r_e$, from $z = 0$ to $52 r_e$. To compute far-field noise spectra and directivities, the LES near-field fluctuations obtained on these control surfaces are propagated to 80 radii from the nozzle exit, by solving the full Euler equations. The same numerical methods as those in the LES, including the shock-capturing procedure [44], are implemented. The grid used for the far-field extrapolation is uniform and contains $800 \times 128 \times 2042 = 209 \times 10^6$ points. The mesh spacings are $\Delta r = 0.1 r_e$ in the radial direction and $\Delta z = 0.074 r_e$ in the axial direction. The numerical cutoff Strouhal number for acoustic propagation is thus around $St_c = 2 f_c r_e / u_e = 1.37$, where $f_c = c_\infty / (4 \Delta r)$. In the present work, the full Euler equations are used for the wave extrapolation in order to take into account the nonlinear effects on acoustic propagation. These effects are illustrated in the Appendix.

III. Instantaneous Fields

Snapshots of azimuthal vorticity, density gradient norm, and fluctuating pressure p' are presented in Fig. 2a, for $z/r_e \leq 15$ and $-3 \leq r/r_e \leq 3$, and in Fig. 2b for the entire flowfield. Near the nozzle exit, the shock-cell structure is displayed using the density gradient norm in Fig. 2a. The first shock cell is static, and slip lines resulting from shock–shock interactions [53] are noticed at the end of the second shock on the jet axis around $z = 7 r_e$. Shocks and compression waves are unsteady downstream of $r = 9 r_e$. At the nozzle exit, the shear layer contracts because of the jet over-expansion. The development of the turbulence and the growth of the shear layer are observed in Fig. 2a. Further downstream at $z > 25 r_e$, the jet plume is seen to be turbulent in Fig. 2b. Concerning the pressure field, waves of high amplitude, first attached to the shear layer in Fig. 2a, appear to radiate in the downstream direction with a conical-wave structure in Fig. 2b. Finally, acoustic waves of lower amplitude are found to propagate in the upstream direction in Fig. 2b.

IV. Aerodynamic Results

A. Mean Flow

The properties of the jet mean flowfield are first investigated and compared with experimental data available in the literature. The variations of the inverse of the mean centerline velocity u_{axis} and of the jet half-width $\delta_{0.5}$ are plotted in Fig. 3. The jet half-width is defined by $\langle u_z \rangle (\delta_{0.5}) = 0.5 u_{\text{axis}}$, where $\langle u_z \rangle$ is the mean axial velocity. The ends of the potential core and of the sonic core are found here when $u_{\text{axis}} = 0.9 u_e$ and c, where c is the local sound speed. They are, respectively, located at $z = 20 r_e$ and $36 r_e$ from the nozzle exit. For comparison, in the similar jet considered using the MARTEL experimental facility [9], the potential core and the sonic core end around 24 and 50 radii. The discrepancies between the computational and experimental core lengths may be explained by the differences in Reynolds number [54] and in initial conditions [37]. The shock-cell structure is, moreover, seen to modulate the jet half-width in the core region. Downstream of the potential core, the mean flow develops rapidly, and the variations of u_e / u_{axis} and $\delta_{0.5} / r_e$ are approximately linear.

The variations of the centerline mean static pressure $\langle p \rangle$ are plotted in Fig. 4a. Six shock cells resulting from the adaptation of the jet exit conditions to the ambient field conditions are noticed. The axial mean static pressure is also compared with measurements by Norum

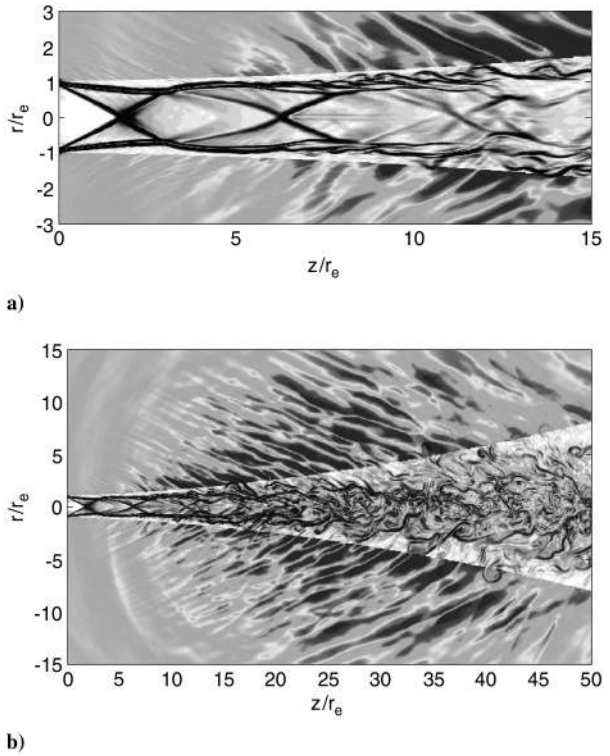

Fig. 2 Snapshots in the (z, r) plane: a) density gradient norm in the jet and fluctuating pressure p' outside the jet and b) density gradient norm and azimuthal vorticity in the jet, and fluctuating pressure p' in grayscale outside the jet. The grayscale ranges for levels from −5000 to 5000 Pa for p', and distances have been normalized by the nozzle radius r_e.

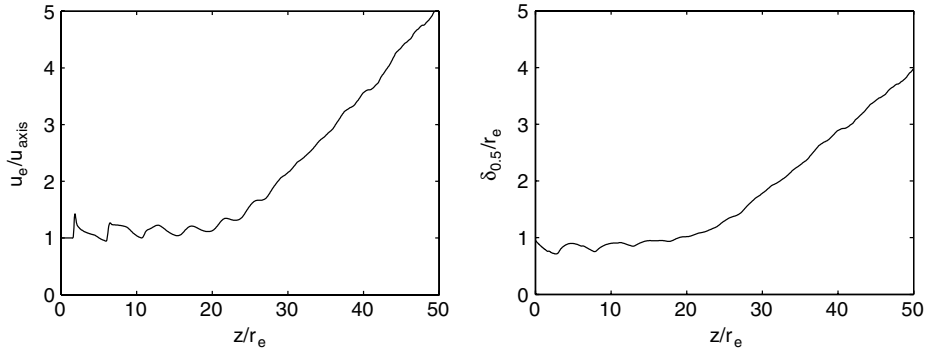

Fig. 3 Variations of a) the inverse of the mean longitudinal velocity u_{axis} along the jet centerline and b) the jet half-width $\delta_{0.5}$.

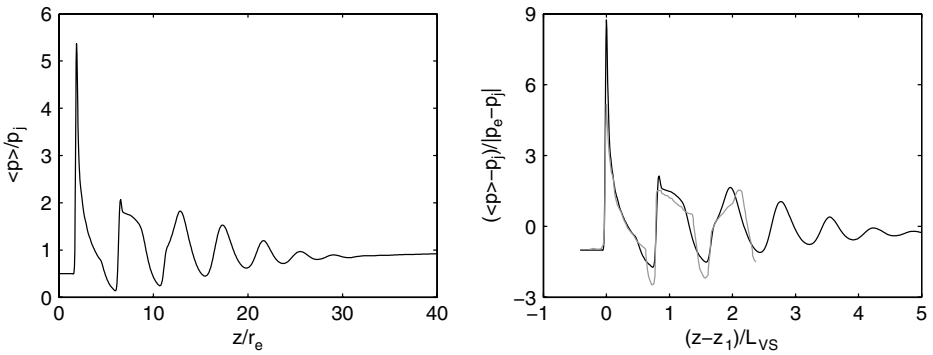

Fig. 4 Variations of the mean static pressure along the jet centerline as a function a) of the axial position z/r_e and b) of $(z - z_1)/L_{VS}$, where z_1 and L_{VS} are the location of the first shock and the length of the first shock cell given by Tam and Tanna's [47] model: present jet (black) and measurements by Norum and Seiner [55] (gray) (refer to Table 2).

and Seiner [55] in Fig. 4b. The overexpanded jet of these authors has an exit Mach number of $M_e = 2$. For the comparison, a scaling proposed by Tam and Tanna [47] is used. The pressure profiles are thus represented as a function of $(z - z_1)/L_{VS}$, where z_1 is the location of the first shock on the jet axis, and L_{VS} is the length of the first shock cell provided by the vortex sheet model of Tam and Tanna [47]. These profiles are normalized by the difference $|p_e - p_j|$ between static pressures at the nozzle exit and at the ambient field. The quantities used for the normalization are given in Table 2. The shapes of the shocks in the computed jet and in the experiment correspond fairly well, despite different exit conditions. For completeness, the measured length L_1 of the first shock cell is also provided in Table 2. It is interesting to note that $L_1 \simeq 0.82L_{VS}$ for both cases.

B. Turbulent Flow

The turbulent flowfield of the present jet is now studied, which will allow us to discuss noise sources in the next section. The root-mean-square (rms) variations of axial, azimuthal, and radial velocities at $r = 0$ and r_j are first plotted in Fig. 5. Along the centerline in Fig. 5a, the amplitude of velocity fluctuations appears to increase in successive stages in the jet core. The maxima of the rms quantities are reached around $z = 25r_e$. They are, respectively, around 18 and 11% of the jet inflow velocity for the axial and radial velocities. Along the shear layer in Fig. 5b, very low rms turbulence levels are found in the vicinity of the nozzle, as expected for an initially laminar jet. The amplitudes of velocity fluctuations then grow, quite sharply around $z = 6.5r_e$ for the axial velocity, but more smoothly for the other components. Consequently, the peak rms values are much higher for the axial velocity, which may also be strengthened by compressible effects [56]. The peak positions, moreover, differ significantly, from about $z = 12r_e$ for the axial velocity, that is, before the end of the potential core, to $z \simeq 25r_e$ for the other velocity components, just downstream of the jet core.

Table 2 Data used for the normalization of the results from the LES and from the experiment of Norum and Seiner [55]

Study	M_e	M_j	$\lvert p_e - p_j \rvert$	L_1	L_{VS}
Present computation	3.30	2.83	0.5×10^5 Pa	$4.6r_e$	$5.6r_e$
Norum and Seiner [55]	2	1.82	0.2×10^5 Pa	$3r_e$	$3.7r_e$

A two-dimensional Fourier transform in time and in the azimuthal direction is now applied to the fluctuating axial velocity u'_z along the line at $r = r_j$. The resulting two-side power spectral densities (PSDs) $|\hat{u}_z|^2(St_e, n)$ depend on the Strouhal number $St_e = 2fr_e/u_e$, where f is the frequency, and on the azimuthal mode n, where n is an integer. This kind of decomposition has previously been carried out for supersonic jets [57,58], in particular to compare numerical results with linear stability analyses. The contribution of the nth mode to the mean-square axial velocity fluctuations $\langle u'^2_z \rangle$ is denoted by $\langle u'^2_z \rangle_n$ next. They are computed by integrating the quantity $|\hat{u}_z|^2(St_e, n)$ over the whole range of Strouhal numbers.

The contributions of modes $n = 0$, 1, and 2 and of higher azimuthal modes are plotted in Fig. 6. The contribution of modes $n > 2$ is dominant upstream of $z = 22r_e$, whereas that of mode $n = 1$ is the largest further downstream. More precisely, the contribution of modes $n > 2$ increases very rapidly in the early stage of the shear-layer development and then decreases downstream of $z \simeq 12r_e$. The contributions of modes $n = 0$, 1, and 2 are initially significantly lower. They also reach maximum values further downstream: around $z \simeq 20r_e$ for mode $n = 2$, $z \simeq 24r_e$ for mode $n = 1$, and $z \simeq 28r_e$ for mode $n = 0$. In the latter case, for the axisymmetric mode, the peaks are, moreover, of much lower amplitude than for the modes $n = 1$ and 2. This difference of amplitude between modes $n = 1$ and

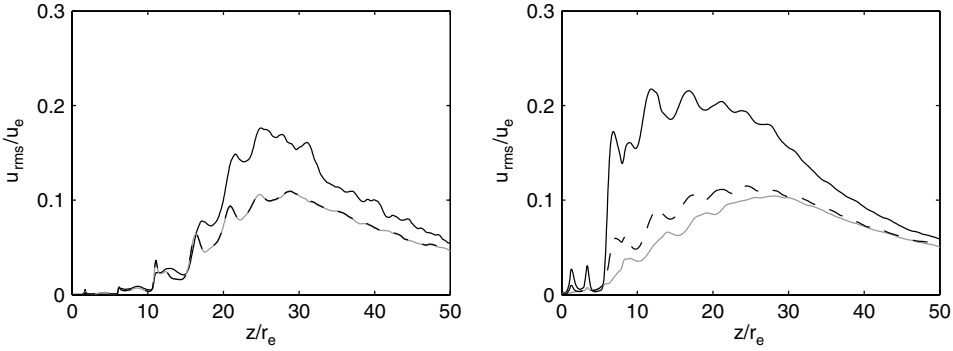

Fig. 5 Variations of rms velocity fluctuations: axial velocity (black solid), azimuthal velocity (dashed), and radial velocity (gray solid) along a) the jet centerline and b) the line $r = r_j$.

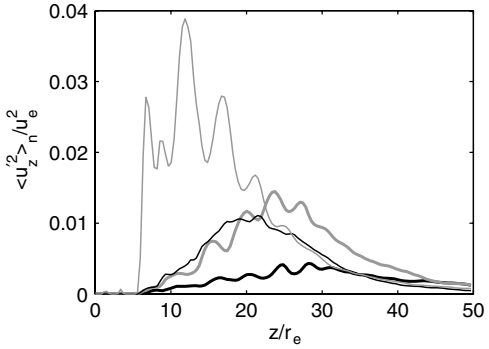

Fig. 6 Axial evolution along the line $r = r_j$ of the azimuthal components of the mean-square value of the fluctuating axial velocity: contributions of axisymmetric component $n = 0$ (thick black), $n = 1$ component (thick gray), $n = 2$ component (black), and azimuthal modes of order higher than two (gray).

2 and the axisymmetric mode agrees with the linear stability analysis performed by Tam et al. [59] and Seiner et al. [60]. In perfectly expanded heated jets at an exit Mach number of $M_j = 2$, these authors indeed found that the amplification along the shear layer of the Kelvin–Helmholtz modes $n = 1$ and 2 are rather close, and that they are stronger than the amplification of the axisymmetric mode.

The features of the axial velocity fluctuations just downstream the nozzle exit at $r = r_j$ and $z = 0.05r_e$ are checked. The velocity spectrum thus obtained, scaled by u_e^2, is presented in Fig. 7a as a function of the Strouhal number St_e. It is broadband and contains no distinct peak. The relative contributions of azimuthal modes n to the fluctuating velocity field are also shown in Fig. 7b. Significant components are found over a wide range of modes, up to $n \simeq 15$. The numerical setup in the present computation therefore does not appear to force a specific jet mode.

The overall PSDs of the axial velocity fluctuations are shown in Fig. 8 along the line at $r = r_j$, at the positions $z = 6.5r_e$, $12r_e$, $18r_e$, $24r_e$, and $30r_e$ from the nozzle exit. They are plotted in logarithmic scales, and for clarity their levels are incremented by one order of magnitude as the axial position increases. At $z = 6.5r_e$, a peak is noticed at Strouhal number $St_e = 0.30$, whereas spectra are more broadband further downstream.

The variations along the shear layer of the peak Strouhal numbers in the spectra of the axial fluctuating velocity are provided in Fig. 9a. Strouhal numbers of 0.30, 0.11, and 0.05 are found. The former peak frequency at $St_e = 0.30$ is dominant over a first stage between $z = 6r_e$ and $9r_e$, where, according to Fig. 6, the azimuthal components of order higher than two are the strongest components. A second stage characterized by a peak frequency at $St_e = 0.11$ is obtained between $z = 12.5r_e$ and $20.5r_e$. At this position, the peak Strouhal number finally switches to a value close to 0.05. A similar shift in frequency near the end of the potential core, from the screech fundamental frequency down to the mixing noise frequency, was evidenced in a plane screeching jet by Berland et al. [22].

Considering the large contribution of the mode $n = 1$ to the axial velocity fluctuations along the shear layer in Fig. 6, the peak Strouhal numbers obtained in the azimuthal spectra $|\hat{u}_z|^2(St_e, n = 1)$ at $r = r_j$ are represented in Fig. 9b. For this mode, $n = 1$, the Strouhal number $St_e = 0.08$ also appears clearly.

V. Acoustic Results

A. Acoustic Near Field

The overall sound pressure levels (OASPL) obtained at $r = 9.5r_e$ and $16r_e$ from the jet centerline are first presented in Fig. 10. At $r = 9.5r_e$ in Fig. 10a, the OASPL increase rapidly from $z = 0$ to $20r_e$, and the maximum of the pressure levels is reached at the axial location $z = 30r_e$. The sound levels obtained at $r = 16r_e$ are compared with Varnier and Gély's [9] measurements in Fig. 10b. They are lower from $z = 0$ to $17r_e$ and higher downstream of

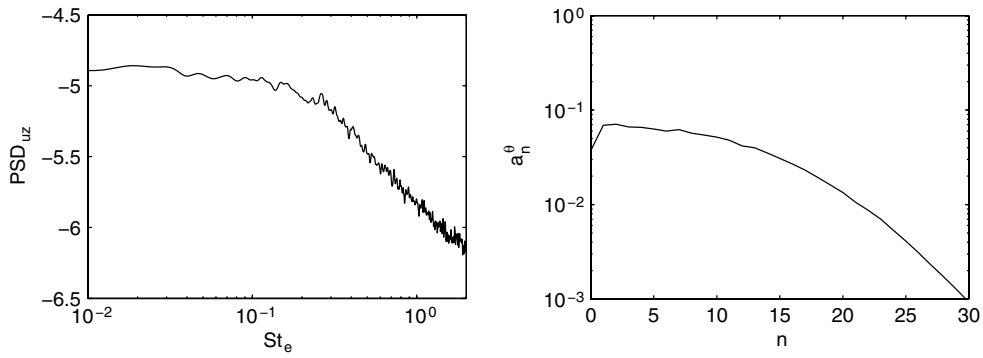

Fig. 7 Axial velocity fluctuations at $r = r_j$ and $z = 0.05r_e$: a) overall PSDs in logarithmic scales and b) relative contribution of azimuthal modes n.

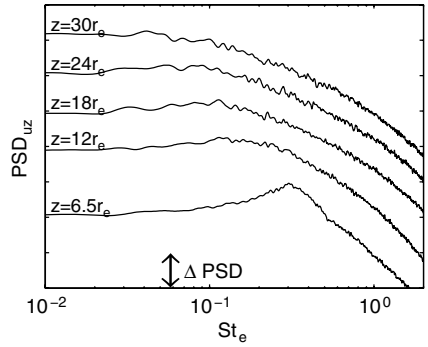

Fig. 8 Overall PSDs in logarithmic scales of the axial velocity fluctuations along the line $r = r_j$ at $z = 6.5$, 12, 18, 24, and $30r_e$. For clarity, the levels are incremented by ΔPSD with the axial distance, where ΔPSD denotes 1 order of magnitude.

$z = 17r_e$, with a discrepancy of 5 dB near the OASPL peak at $z \simeq 35r_e$. This may result from differences in nozzle-exit conditions [37,61], as well as in Reynolds number [54,62]. The Reynolds number in the LES is indeed 0.94×10^5, whereas it is 17.5×10^5 in the experiment. Various sound pressure levels may consequently be expected, according to the observations of Troutt and McLaughlin [54], for Mach-number-2 jets at Reynolds numbers 0.7×10^5 and 52×10^5.

The relative contributions of azimuthal modes $n = 0$, 1, 2, and $n > 2$ to the fluctuating pressure at $r = 9.5r_e$ are shown in Fig. 11 as a function of the axial position z/r_e. From $z = 0$ to $30r_e$, the mode $n = 1$ clearly dominates the acoustic near field, except for the region between $z = 8r_e$ and $18r_e$, over which the contribution of higher modes $n > 2$ appears as important. The relative amplitude of the mode $n = 0$ becomes equal to that of the mode $n = 1$ around the position $z = 30r_e$, where the OASPL peak is observed in Fig. 10a. Downstream of this location, the axisymmetric component is predominant. The contribution of the mode $n = 2$ to the radiated sound field is maximum around $z/r_e \simeq 15$, but it is rather low everywhere else. Note that the present results, in particular the relative dominance of the modes $n = 0$ and 1 in the acoustic near field, are satisfactorily consistent with the numerical results obtained by Bodony et al. [63] at $r = 10r_e$ for an underexpanded jet at a Mach number of $M_e = 1.95$.

Acoustic near-field spectra are displayed in Fig. 12 at $r = 9.5r_e$ and $z = 0$, $10r_e$, $15r_e$, and $20r_e$. They are computed using fast Fourier transforms over eight overlapping data samples of duration $T = 289r_e/u_e$ containing 2850 points. The spectra are also averaged in the azimuthal direction. The spectrum at $z = 0$ is dominated by two components at $St_e = 0.08$ and 0.10. The former component is also noticed in the spectra at $z = 10r_e$, $15r_e$, and $20r_e$ at the same frequency, whereas the latter one moves toward higher Strouhal numbers with the axial position following the dashed line plotted in Fig. 12. At $z = 0$, the spectrum also exhibits a low-frequency peak around $St_e = 0.05$, and at $z = 10r_e$ and $15r_e$ a broadband high-frequency noise component centered around $St_e = 0.30$ is also visible.

To first give information on noise sources, the peak frequency predicted by the model proposed by Tam et al. [23] for the upstream-propagating shock-associated jet noise associated with possible screech is represented in Fig. 12. This expression is written as

$$f_{\text{up}} = \frac{u_c}{L_{\text{shock}}(1 + M_c)} \tag{1}$$

where u_c is the convection velocity, $M_c = u_c/c_\infty$ is the convection Mach number, and L_{shock} is the mean shock-cell length, which is here taken equal to L_1. From axial velocity cross correlations determined in the jet between $z = 6r_e$ and $20r_e$ along the shear layer at $r = r_j$, the

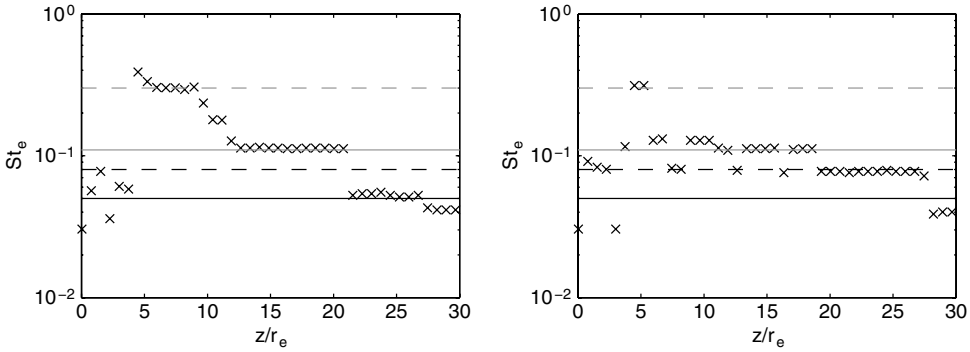

Fig. 9 Peak Strouhal numbers (x) along the line $r = r_j$ in the PSDs of the axial velocity fluctuations: a) overall spectra and b) spectra for the $n = 1$ azimuthal component. The lines represent $St_e = 0.05$ (black), $St_e = 0.08$ (black dashed), $St_e = 0.11$ (gray), and $St_e = 0.30$ (gray dashed).

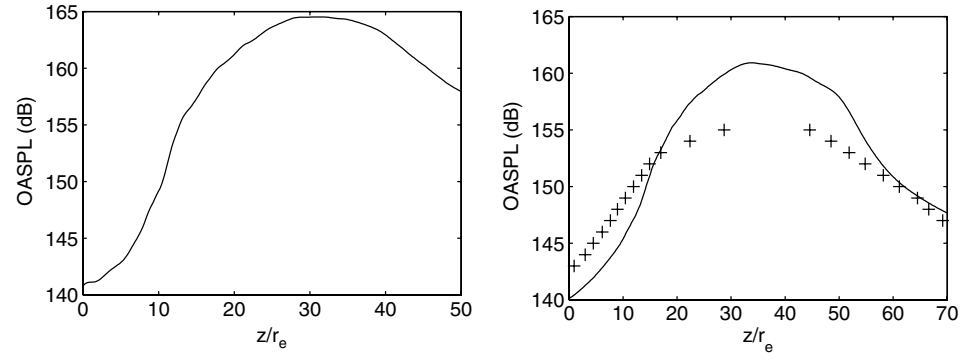

Fig. 10 Variations of the OASPLs: a) computational results at $r = 9.5r_e$ and b) computational results (line) and measurements of Varnier and Gély [9] (+) at $r = 16r_e$.

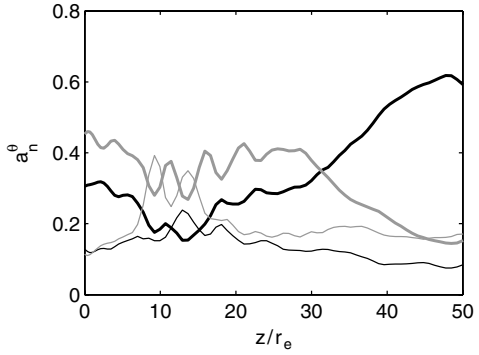

Fig. 11 Variations in the axial direction of the relative contributions a_n^θ of azimuthal modes n to the fluctuating pressure at $r = 9.5r_e$: axisymmetric mode $n = 0$ (thick black), mode $n = 1$ (thick gray), mode $n = 2$ (black), and modes of order higher than two (gray).

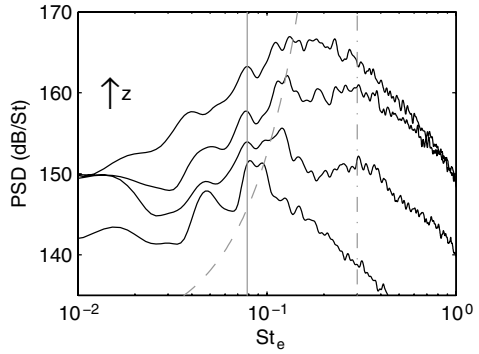

Fig. 12 Near-field acoustic spectra at $r = 9.5r_e$. From bottom to top: $z = 0$, $10r_e$, $15r_e$, and $20r_e$; frequency predicted for the upstream-propagating shock-associated noise using Eq. (1) (solid gray), $St_e = 0.30$ (dashed–dotted gray), and moving peak frequency (dashed gray).

average convection velocity has been estimated as $u_c = 0.53u_e$. Equation (1) thus yields Strouhal number $St_{\text{up}} = 2r_e f_{\text{up}}/u_e = 0.08$, which agrees with the frequency of the persistent noise component observed in the spectra of Fig. 12. This component can therefore be associated with upstream-propagating shock-associated noise. Regarding the peak frequency moving from $St_e \approx 0.10$ at $z = 0$ to $St_e \approx 0.13$ at $z = 20r_e$, a similar feature has been found in near-field measurements by Seiner and Yu [20] for an overexpanded jet at Mach number 1.45. According to these authors, it can be identified as the central frequency of the broadband shock-associated noise.

Acoustic spectra of azimuthal modes $n = 0$, 1, 2, and $n > 2$ are presented in Fig. 13 at $r = 9.5r_e$ and $z = 0$ and $10r_e$. At $z = 0$ in Fig. 13a, the maximum in the spectrum for the mode $n = 0$ is noticed at $St_e = 0.05$. A peak of lower magnitude also appears at $St_e = 0.10$, which corresponds to the first harmonic of the previous frequency. The maximum in the spectrum for the mode $n = 1$ is stronger and is observed at $St_e = 0.08$. For this mode, a second peak seems to emerge at $St_e = 0.10$. Consequently, the peak at $St_e = 0.05$ and the peaks at $St_e = 0.08$ and 0.10 observed at $z = 0$ in Fig. 12 can be associated, respectively, with the modes $n = 0$ and 1. In Fig. 13a, the peak component in the spectrum for the mode $n = 2$ is now quite low, with respect to previous peaks, and is reached for $St_e = 0.15$. The modes $n > 2$ are also found to contribute negligibly to the acoustic near field at $z = 0$ for Strouhal number lower than 0.2, but predominantly for higher frequencies.

For the mode $n = 0$, the peaks observed at $St_e = 0.05$ and 0.10 in Fig. 13a at $z = 0$ have moved to $St_e = 0.07$ and 0.12 in Fig. 13b at $z = 10r_e$. For the mode $n = 1$, two distinct peaks of similar magnitude are seen. The first one is at $St_e = 0.08$, as in the spectrum at $z = 0$, and the second one is at $St_e = 0.12$, which coincides with the maximum frequency in the spectrum for $n = 0$. These results suggest that the peak found at $St_e = 0.08$ in the acoustic spectrum at $z = 10r_e$ in Fig. 12 is connected to the mode $n = 1$, but also that the moving peak is linked both to modes $n = 0$ and 1. In Fig. 13b, as seen previously, the contribution of modes $n > 2$ is moreover dominant for $St_e \geq 0.2$. It is characterized by a broadband shape and a maximum around $St_e = 0.30$, and its level is very close to the peak levels obtained in the spectra for modes $n = 0$ and 1. The high-frequency components in the acoustic spectra at $z = 10r_e$ are then clearly associated with modes $n > 2$.

Some connections between peaks at $St_e = 0.05$, 0.08, and 0.30 in the velocity spectra in Fig. 9 and in the near-field acoustic spectra in Fig. 12 can be emphasized. Concerning $St_e = 0.08$, peaks are found at this frequency in the near pressure fields at different axial locations, and they are associated with the mode $n = 1$. This frequency also emerges in the velocity spectra calculated along the shear layer for the mode $n = 1$ in Fig. 9b. A similar behavior has been described by Berland et al. [22] in a plane screeching jet at the screech tone frequency. Therefore, the noise component at $St_e = 0.08$ in the present jet appears to be upstream-propagating shock-associated noise.

The axisymmetric noise component found at $St_e = 0.05$ in the near pressure field at $z = 0$, in Fig. 12, corresponds well with that experimentally noticed at a frequency lower than the screech tone frequency in upstream acoustic spectra [24,64] of screeching jets. According to Tam [19], it can then be identified as turbulent mixing noise. This may be supported by the observation in Fig. 9a that dominant velocity components downstream of the potential core are also at $St_e = 0.05$.

Finally, to track the origin of the broadband noise components centered around $St_e = 0.30$ found at $z = 10$ and $15r_e$ in Fig. 12, it is interesting to point out that in Fig. 9a $St_e = 0.30$ predominates in the velocity spectra computed between $z = 6$ and $9r_e$ along the shear layer. The link is strengthened by the fact that corresponding fluctuations in both cases are associated with azimuthal modes $n > 2$. This broadband high-frequency noise therefore appears to be generated in the early development of the shear layer. Because it is

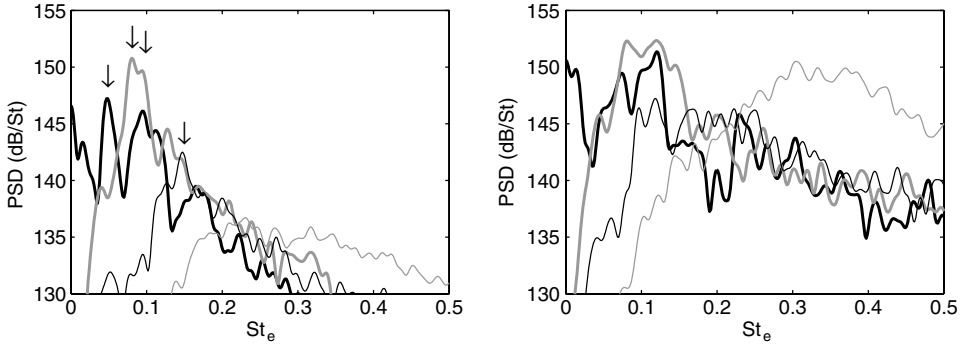

Fig. 13 Acoustic spectra of azimuthal modes at a) $(r, z) = (9.5r_e, 0)$ and b) $(r, z) = (9.5r_e, 10r_e)$: mode $n = 0$ (thick black), mode $n = 1$ (thick gray), mode $n = 2$ (black), and modes of order higher than two (gray). The arrows represent $St_e = 0.05$, 0.08, 0.10, and 0.15.

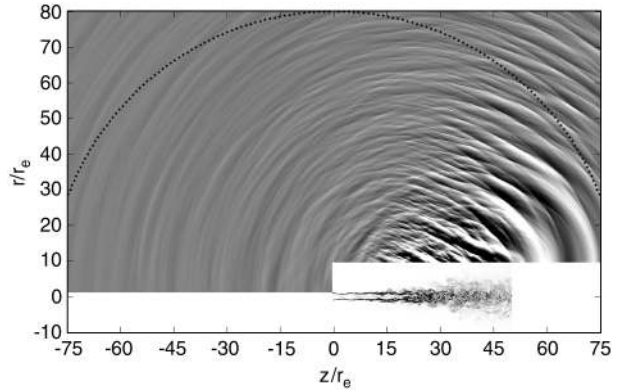

Fig. 14 Snapshot in the (z, r) plane of the fluctuating pressure obtained from the far-field wave extrapolation. The gray scale ranges for levels from −2000 to 2000 Pa. Pressure signals are recorded along the dotted circular arc.

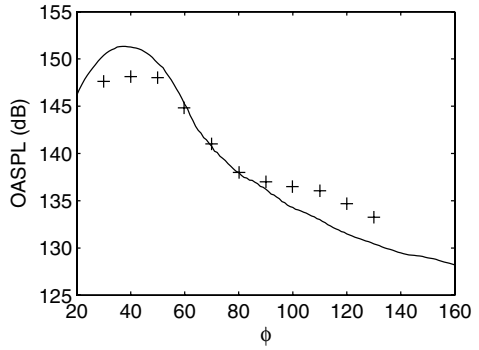

Fig. 15 OASPLs as a function of the angle ϕ with respect to the jet direction at $80r_e$ from the nozzle exit: computation (line) and measurements of Robin [10] (+).

not distinguished in the near pressure field at $z = 0$ in Fig. 12, it can reasonably be attributed to a Mach-wave radiation.

B. Acoustic Far Field

The LES data recorded on the control surfaces located, respectively, at $r = 9.5r_e$ and at $z = 0$, as mentioned in Sec. II.B, are propagated to 80 radii from the nozzle exit. For this, the full Euler equations are solved using the same methods as those in the LES, including the shock-capturing procedure [44], in order to take into account the nonlinear propagation of sound waves in high-speed jets [30,65,66]. A snapshot of the computed fluctuating pressure is represented in Fig. 14. The overexpanded jet radiates mainly in the downstream direction, but upstream-propagating waves are also noticed. Far-field acoustic spectra calculated using linear and nonlinear equations for the wave extrapolation are provided in the Appendix to show the importance of nonlinear effects.

The sound pressure levels at $80r_e$ from the nozzle exit are presented in Fig. 15 as a function of the radiation angle ϕ, where ϕ is measured according to the flow direction. The maximum level is reached in the downstream direction around $\phi = 40°$. The present acoustic levels are compared with experimental data obtained at the same distance by Robin [10] for an overexpanded, Mach number 3.13 jet characterized by stagnation pressure and temperature of 30×10^5 Pa and 1900 K. The computation provides higher sound levels in the downstream direction and lower levels in the upstream direction.

The spectra of the pressure p' at 80 radii from the jet exit are represented in Fig. 16 as a function of the Strouhal number St_e and the angle ϕ. In the downstream direction in Fig. 16a, for $\phi \leq 80°$, two distinct noise components are observed at frequencies around $St_e = 0.05$ and 0.10. The first one is found to mainly radiate from $\phi = 26$ to 36°, and the second one is especially strong from $\phi = 37$ to 43°. In the sideline and upstream radiation directions in Fig. 16b, the peak Strouhal number in the acoustic spectra decreases with the angle ϕ. It is shown to agree well with the central frequency of the broadband shock-associated noise:

$$f_{\text{shock}} = \frac{u_c}{L_{\text{shock}}[1 - M_c \cos(\phi)]} \tag{2}$$

proposed by Tam and Tanna [47], also displayed in Fig. 16b in a dashed black line. This indicates the predominance of shock-associated noise in the upstream direction.

Far-field pressure spectra at $\phi = 30, 40, 90$, and 120° are shown in Fig. 17. At $\phi = 30$ and 40° in Fig. 17a, the spectra have narrow shapes, and contain significant noise components at low frequencies. The maxima in the spectra are, respectively, at $St_e = 0.05$ and 0.10. These results are consistent with measurements of Seiner et al. [60] for heated jets at Mach number 2. In the sound spectrum at $\phi = 90°$ in Fig. 17b, two peaks at $St_e = 0.16$ and 0.20 are noticed. These Strouhal numbers correspond to the first harmonics of the peak frequencies observed at $St_e = 0.08$ and 0.10 in near field at $z = 0$ in Fig. 12, which have been identified as upstream-propagating shock-associated noise components. This corresponds to the behavior of screeching jets, in which the first harmonic of the screech tone is usually dominant in the sideline direction [22,67]. Finally, at $\phi = 120°$, the maximum sound level is obtained at $St_e = 0.11$, which agrees well with Tam and Tanna's [47] prediction [Eq. (2)] of the central frequency of the broadband shock-associated noise. The spectra of Fig. 17b therefore support the predominance of shock-associated noise both in the sideline and the upstream directions.

To discuss the nature of the noise components in the downstream direction, the far-field pressure spectra for the axisymmetric mode and the mode $n = 1$ are plotted in Fig. 18 for $\phi \leq 80°$. For the mode $n = 0$ in Fig. 18a, peaks are observed at $St_e = 0.05$ and 0.10, whereas, for the mode $n = 1$ in Fig. 18b, only $St_e = 0.08$ dominates.

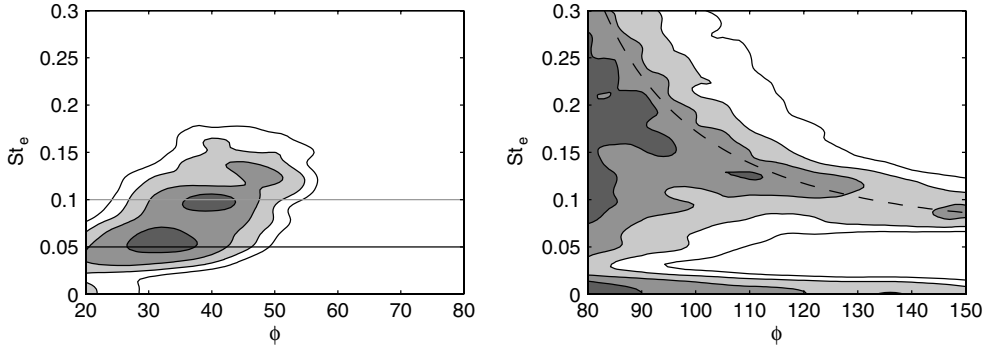

Fig. 16 PSDs of pressure as a function of the angle ϕ and the Strouhal number St_e: a) from $\phi = 20$ to 80° and b) from $\phi = 80$ to 150°; the gray scales range a) from 154 to 162 dB/St and b) from 135.5 to 143.5 dB/St; $St_e = 0.05$ (black line), $St_e = 0.10$ (gray line), and central frequency of the broadband shock-associated noise predicted [47] using Eq. (2) (dashed).

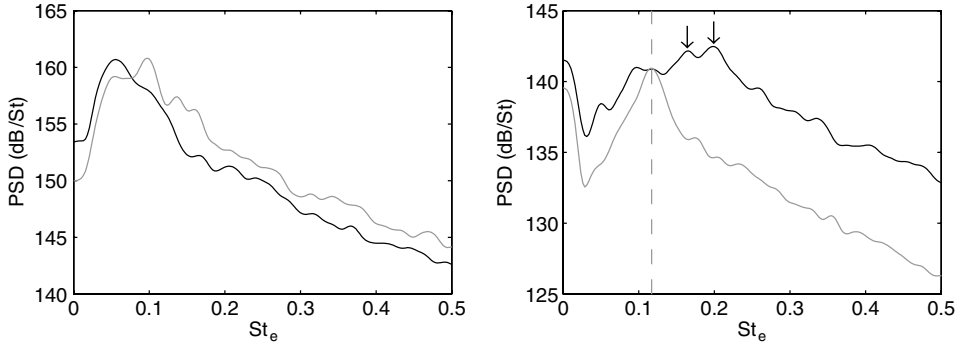

Fig. 17 Far-field pressure spectra a) at $\phi = 30°$ (black) and $\phi = 40°$ (gray) and b) at $\phi = 90°$ (black) and $\phi = 120°$ (gray); peak frequency of the broadband shock-associated noise predicted [47] using Eq. (2) at $\phi = 120°$ (dashed). The arrows represent $St_e = 0.16$ and 0.20.

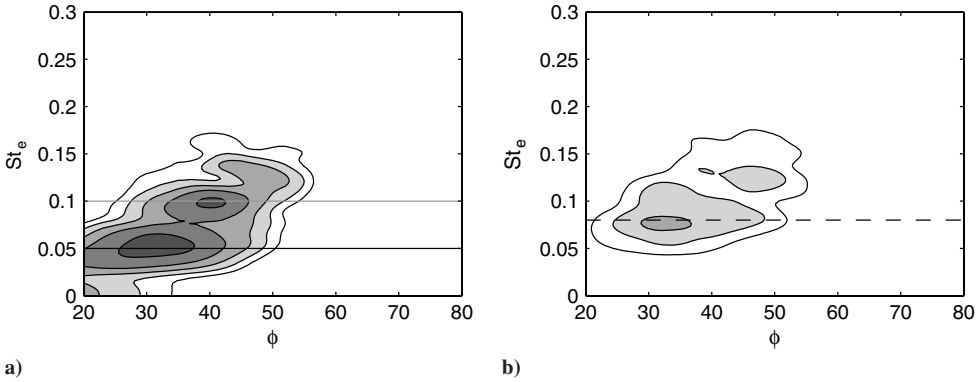

Fig. 18 Far-field pressure spectra for modes a) $n = 0$ and b) $n = 1$ as a function of the angle ϕ and the Strouhal number St_e, for $\phi \leq 80°$. The gray scale ranges from 151 to 161 dB/St; $St_e = 0.05$ (black line), $St_e = 0.10$ (gray line), and $St_e = 0.08$ (dashed).

The noise components at $St_e = 0.05$ and 0.10 in the spectra in Fig. 16a are therefore connected to the mode $n = 0$. Note that very similar frequencies have been shown in Fig. 9a to emerge in the axial velocity spectra along the shear layer: $St_e = 0.11$ from the end of the second shock cell to the end of the potential core and $St_e = 0.05$ downstream of the jet core. According to its azimuthal distribution, the noise component at $St_e = 0.05$ can thus be identified as turbulent mixing noise generated downstream of the potential core. The noise component at $St_e = 0.10$ may be related to the velocity fluctuations at $St_e = 0.11$ in the shear layer. Its generation mechanism is unfortunately currently unclear.

As mentioned previously, for the mode $n = 1$, acoustic disturbances of maximum amplitude are found in Fig. 18b around $St_e = 0.08$, between $\phi = 30$ and 40°. Significant axial velocity fluctuations have also been displayed in Fig. 9b along the shear layer, at the same Strouhal number for the same mode. The noise component at $St_e = 0.08$ could therefore be generated by Mach-wave mechanisms.

Finally, the azimuthal decomposition into modes $n = 0$ and 1 is applied to the sideline and upstream acoustic far field in Fig. 19. The sound levels are higher in Fig. 19b, which first suggests that shock-associated noise is mainly connected to the mode $n = 1$. In Fig. 19a, for the axisymmetric mode, two peaks at $St_e = 0.05$ and 0.10 appear at $\phi = 150°$. They have been previously associated, respectively, with turbulent mixing noise and shock-associated noise at the end of the Sec. V.A. A peak at $St_e = 0.20$, which corresponds to the first harmonic of the peak frequency at $St_e = 0.10$, is also observed at $\phi = 90°$. In Fig. 19b, for the mode $n = 1$, a first shock-associated noise component emerges at $\phi = 150°$ around $St_e = 0.08$, while a second one can be distinguished at $\phi = 90°$ at the first harmonic

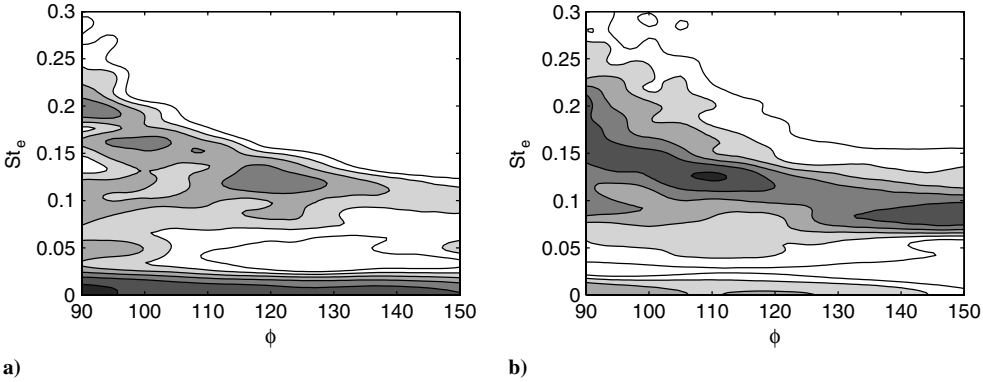

Fig. 19 Far-field pressure spectra for modes a) $n = 0$ and b) $n = 1$ as a function of the angle ϕ and the Strouhal number St_e, for $\phi \geq 90°$. The gray scale ranges from 129.5 to 139.5 dB/St.

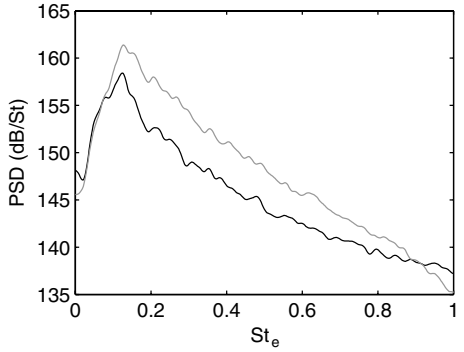

Fig. 20 Far-field sound spectra obtained from the LES near field, at $80r_e$ from the nozzle exit and at $\phi = 50°$, by solving the linear acoustic equations (gray) and the full Euler equations (black).

frequency. It is, finally, interesting to note that the central frequency of the upstream shock-associated noise varies with the mode, from $St_e = 0.10$ for the mode $n = 0$ to $St_e = 0.08$ for $n = 1$.

VI. Conclusions

In the present study, a compressible three-dimensional LES is performed for an initially laminar overexpanded jet at an exit Mach number of 3.30 and an exit temperature of 360 K, using low-dissipation schemes and an adaptive shock-capturing procedure. The jet flowfield, the pressure near field, and the acoustic far field obtained using the Euler equations are described. Comparisons are made with available measurements and with models. Noise sources in the present jet are discussed by characterizing the properties of the axial velocity fluctuations along the shear layer and of acoustic disturbances. In this way, some links are shown between the aerodynamic and the sound fields. Contributions of shock-associated noise, Mach waves, and turbulent mixing noise to the acoustic spectra are identified. This study thus constitutes a first step in the study of highly supersonic jets before dealing with realistic nozzle geometries or exit turbulent conditions. In the latter case, in particular, a much finer discretization of the jet boundary layers would be necessary [36].

Appendix: Influence of Nonlinear Propagation Effects

Nonlinear propagation effects of acoustic waves may be significant for supersonic jets [30,65,66]. In this Appendix, the importance of these effects during the sound propagation from the jet near field to the acoustic far field is therefore evaluated for the considered jet. Two far-field wave extrapolations are performed from the LES data over control surfaces at $z = 0$ and $r = 9.5r_e$, one by solving the linear acoustic equations and another by solving the full Euler equations, on the same grid using identical numerical methods. The spectra thus obtained at $80r_e$ from the nozzle exit and at $\phi = 50°$ are presented in Fig. 20 as a function of the Strouhal number St_e. They are found to differ appreciably for $St_e > 0.08$. The noise levels computed using the full Euler equations are, in particular, lower than those obtained using the linear equations for Strouhal numbers $St_e < 0.9$ (by 3 dB, for instance, at the peak frequency around $St_e = 0.13$), and they are higher for $St_e > 0.9$. These results indicate that nonlinear propagation effects must be here taken into account to predict noise at medium and high frequencies.

Acknowledgments

The work presented in this paper is sponsored by Centre National d'Etudes Spatiales. The authors would like to thank the task monitor Hadrien Lambaré for his support. This work was granted access to the high-performance computing resources of the Institut du Développement et des Ressources en Informatique Scientifique under the allocation 2010-020204 made by Grand Equipement National de Calcul Intensif.

References

[1] Varnier, J., "Experimental Study and Simulation of Rocket Engine Free Jet Noise," *AIAA Journal*, Vol. 39, No. 10, 2001, pp. 1851–1859. doi:10.2514/2.1199

[2] Ffowcs Williams, J. E., and Maidanik, G., "The Mach Wave Field Radiated by Supersonic Turbulent Shear Flows," *Journal of Fluid Mechanics*, Vol. 21, No. 4, 1965, pp. 641–657. doi:10.1017/S0022112065000393

[3] Oertel, H., "Mach Wave Radiation of Hot Supersonic Jets Investigated by Means of the Shock Tube and New Optical Techniques," *Proceedings of the 12th International Symposium on Shock Tubes and Waves*, Jerusalem, 1980, pp. 266–275.

[4] Tam, C. K. W., and Hu, F. Q., "On the Three Families of Instability Waves of High-Speed Jets," *Journal of Fluid Mechanics*, Vol. 201, No. 1, 1989, pp. 447–483. doi:10.1017/S002211208900100X

[5] Bailly, C., Lafon, P., and Candel, S., "Prediction of Supersonic Jet Noise from Statistical Acoustic Model and a Compressible Turbulence Closure," *Journal of Sound and Vibration*, Vol. 194, No. 2, 1996, pp. 219–242. doi:10.1006/jsvi.1996.0354

[6] Krothapalli, A., Arakeri, V., and Greska, B., "Mach Wave Radiation: A Review and an Extension," 41st Aerospace Science Meeting and Exhibit, AIAA Paper 2003-1200, Reno, NV, 2003.

[7] Nonomura, T., and Fujii, K., "Over-Expansion Effects on Mach 3.0 Supersonic Jet Acoustics," 14th AIAA/CEAS Aeroacoustics Conference, AIAA Paper 2008-2836, Vancouver, 2008.

[8] Nonomura, T., and Fujii, K., "Mach Number and Temperature Effects on Mach Wave Emission from Supersonic Jets," 26th AIAA Applied Aerodynamic Conference, AIAA Paper 2008-6587, Honolulu, 2008.

[9] Varnier, J., and Gély, D., "Caractérisation Aérodynamique Et Acoustique D'Un Jet Fortement Supersonique En Présence D'Un Obstacle Plan," ONERA Rept. RT-112/3643, 1998 (not published).

[10] Robin, X., "Contribution Expérimentale À L'Identification Des Sources De Bruit Des Jets Subsoniques Et Supersoniques Chauds," Ph.D. Dissertation, Université de Poitiers, Poitiers, France, 2010.

[11] Panda, J., and Mosher, R., "Use of a Microphone Phased Array to Determine Noise Sources in a Rocket Plume," 49th AIAA Aerospace Sciences Meeting Including the New Horizons Forum and Aerospace Exposition, AIAA Paper 2011-974, Orlando, FL, 2011.

[12] Tam, C. K. W., Viswanathan, K., Ahuja, K. K., and Panda, J., "The Sources of Jet Noise: Experimental Evidence," *Journal of Fluid Mechanics*, Vol. 615, 2008, pp. 253–292. doi:10.1017/S0022112008003704

[13] Tam, C. K. W., Golbiowski, M., and Seiner, J. M., "On the Two Components of Turbulent Mixing Noise from Supersonic Jets," Second AIAA/CEAS Aeroacoustics Conference, AIAA Paper 1996-1716, 1996.

[14] Viswanathan, K., "Analysis of the Two Similarity Components of Turbulent Mixing Noise," *AIAA Journal*, Vol. 40, No. 9, 2002, pp. 1735–1744. doi:10.2514/2.1878

[15] Bogey, C., and Bailly, C., "Investigation of Downstream and Sideline Subsonic Jet Noise Using Large Eddy Simulation," *Theoretical and Computational Fluid Dynamics*, Vol. 20, No. 1, 2006, pp. 23–40. doi:10.1007/s00162-005-0005-7

[16] Panda, J., and Seasholtz, R. G., "Experimental Investigation of Density Fluctuations in High-Speed Jets and Correlation with Generated Noise," *Journal of Fluid Mechanics*, Vol. 450, 2002, pp. 97–130.

[17] Bogey, C., and Bailly, C., "An Analysis of the Correlations Between the Turbulent Flow and the Sound Pressure Field of Subsonic Jets," *Journal of Fluid Mechanics*, Vol. 583, 2007, pp. 71–97. doi:10.1017/S002211200700612X

[18] Tam, C. K. W., and Burton, D. E., "Sound Radiated by Instability Waves of Supersonic Flows. Part 2. Axisymmetric Jets," *Journal of Fluid Mechanics*, Vol. 138, No. 1, 1984, pp. 273–295. doi:10.1017/S0022112084000124

[19] Tam, C., "Supersonic Jet Noise," *Annual Review of Fluid Mechanics*, Vol. 27, No. 1, 1995, pp. 17–43. doi:10.1146/annurev.fl.27.010195.000313

[20] Seiner, J. M., and Yu, J. C., "Acoustic Near-Field Properties Associated with Broadband Shocknoise," *AIAA Journal*, Vol. 22, No. 9, 1984, pp. 1207–1215. doi:10.2514/3.8762

[21] Tanna, H. K., "An Experimental Study of Jet Noise. Part 2: Shock Associated Noise," *Journal of Sound and Vibration*, Vol. 50, No. 3, 1977, pp. 429–444. doi:10.1016/0022-460X(77)90494-1

[22] Berland, J., Bogey, C., and Bailly, C., "Numerical Study of Screech Generation in a Planar Supersonic Jet," *Physics of Fluids*, Vol. 19, No. 7, 2007, p. 075105. doi:10.1063/1.2747225

[23] Tam, C., Seiner, J., and Yu, J., "Proposed Relationship Between Broadband Shock Associated Noise and Screech Tones," *Journal of Sound and Vibration*, Vol. 110, No. 2, 1986, pp. 309–321. doi:10.1016/S0022-460X(86)80212-7

[24] Raman, G., "Cessation of Screech in Underexpanded Jets," *Journal of Fluid Mechanics*, Vol. 336, 1997, pp. 69–90. doi:10.1017/S002211209600451X

[25] Powell, A., "On the Mechanism of Choked Jet Noise," *Proceedings of the Physical Society*, Vol. 66, No. 12, 1953, pp. 1039–1057. doi:10.1088/0370-1301/66/12/306

[26] Alkislar, M. B., Krothapalli, A., and Lourenco, L. M., "Structure of Screeching Rectangular Jet: A Stereoscopic Particle Image Velocimetry Study," *Journal of Fluid Mechanics*, Vol. 489, 2003, pp. 121–154. doi:10.1017/S0022112003005032

[27] Panda, J., "An Experimental Investigation of Screech Noise Generation," *Journal of Fluid Mechanics*, Vol. 378, 1999, pp. 71–96. doi:10.1017/S0022112098003383

[28] Viswanathan, K., "Aeroacoustics of Hot Jets," *Journal of Fluid Mechanics*, Vol. 516, 2004, pp. 39–82. doi:10.1017/S0022112004000151

[29] Seiner, J., Ponton, M., Jansen, B., and Lagen, N., "The Effects of Temperature on Supersonic Jet Noise Emission," 14th AIAA Aeroacoustics Conference, AIAA Paper 1992-2046, Aachen, Germany, 1992.

[30] Viswanathan, K., Alkislar, M. B., and Czech, M. J., "Characteristics of the Shock Noise Component of Jet Noise," *AIAA Journal*, Vol. 48, No. 1, 2010, pp. 25–46. doi:10.2514/1.38521

[31] Massey, K. C., Ahuja, K. K., Jones, R. R., and Tam, C. K. W., "Screech Tones of Supersonic Heated Free Jets," 32nd Aerospace Sciences Meeting and Exhibit, AIAA Paper 1994-0141, Reno, NV, 1994.

[32] Massey, K. C., and Ahuja, K. K., "Screech Frequency Prediction in Light of Mode Detection and Convection Speed Measurements for Heated Jets," Third AIAA/CEAS Aeroacoustics Conference, AIAA Paper 1997-1625, Atlanta, 1997.

[33] Freund J. B., Lele, S. K., and Moin, P., "Numerical Simulation of a Mach 1.92 Turbulent Jet and its Sound Field," *AIAA Journal*, Vol. 38, No. 11, 2000, pp. 2023–2031. doi:10.2514/2.889

[34] Mendez, S., Shoeybi, M., Sharma, A., Ham, F. E., Lele, S. K., and Moin, P., "Large-Eddy Simulations of Perfectly-Expanded Supersonic Jets: Quality Assessment and Validation," 48th AIAA Aerospace Sciences Meeting Including the New Horizons Forum and Aerospace Exposition, AIAA Paper 2010-0271, Orlando, FL, 2010.

[35] Bogey, C., and Bailly, C., "Computation of High Reynolds Number Jet and its Radiated Noise Using Large Eddy Simulation Based on Explicit Filtering," *Computers and Fluids*, Vol. 35, No. 10, 2006, pp. 1344–1358. doi:10.1016/j.compfluid.2005.04.008

[36] Bogey, C., Marsden, O., and Bailly, C., "Large-Eddy Simulation of the Flow and Acoustic Fields of a Reynolds Number 10^5 Subsonic Jet with Tripped Exit Boundary Layers," *Physics of Fluids*, Vol. 23, No. 3, 2011, p. 035104. doi:10.1063/1.3555634

[37] Bogey, C., and Bailly, C., "Influence of Nozzle-Exit Boundary Layer Conditions on the Flow and Acoustic Fields of Initially Laminar Jets," *Journal Fluid Mechanics*, Vol. 663, 2010, pp. 507–538. doi:10.1017/S0022112010003605

[38] Viswanathan, K., Shur, M., Spalart, P. R., and Strelets, M., "Flow and Noise Predictions for Single and Dual-Stream Beveled Nozzles," *AIAA Journal*, Vol. 46, No. 3, 2008, pp. 601–626. doi:10.2514/1.27299

[39] Liu, J. L., Ramamurti, R., Munday, D., Gutmark, E., and Lohoner, R., "Large-Eddy Simulations of a Supersonic Jet and its Near-Field Acoustic Properties," *AIAA Journal*, Vol. 47, No. 8, 2009, pp. 1849–1863. doi:10.2514/1.43281

[40] Lele, S. K., "Compact Finite Difference Schemes with Spectral-Like Resolution," *Journal of Computational Physics*, Vol. 103, No. 1, 1992, pp. 16–42. doi:10.1016/0021-9991(92)90324-R

[41] Tam, C., and Webb, J., "Dispersion-Relation-Preserving Finite Difference Schemes for Computational Aeroacoustics," *Journal of Computational Physics*, Vol. 107, No. 2, 1993, pp. 262–281. doi:10.1006/jcph.1993.1142

[42] Bogey, C., and Bailly, C., "A Family of Low Dispersive and Low Dissipative Explicit Schemes for Flow and Noise Computations," *Journal of Computational Physics*, Vol. 194, No. 1, 2004, pp. 194–214. doi:10.1016/j.jcp.2003.09.003

[43] Pirozzoli, S., "Conservative Hybrid Compact-Weno Schemes for Shock–Turbulence Interaction," *Journal of Computational Physics*, Vol. 178, No. 1, 2002, pp. 81–117. doi:10.1006/jcph.2002.7021

[44] Bogey, C., de Cacqueray, N., and Bailly, C., "A Shock Capturing Methodology Based on Adaptative Spatial Filtering for High-Order Non-Linear Computations," *Journal of Computational Physics*, Vol. 228, No. 5, 2009, pp. 1447–1465. doi:10.1016/j.jcp.2008.10.042

[45] Pirozzoli, S., "On the Spectral Properties of Shock-Capturing Schemes," *Journal of Computational Physics*, Vol. 219, No. 2, 2006, pp. 489–497. doi:10.1016/j.jcp.2006.07.009

[46] Berland, J., Bogey, C., Marsden, O., and Bailly, C., "High-Order, Low Dispersive and Low Dissipative Explicit Schemes for Multi-Scale and Boundary Problems," *Journal of Computational Physics*, Vol. 224, No. 2, 2007, pp. 637–662. doi:10.1016/j.jcp.2006.10.017

[47] Tam, C. K. W., and Tanna, H. K., "Shock Associated Noise of Supersonic Jets from Convergent-Divergent Nozzles," *Journal of Sound and Vibration*, Vol. 81, No. 3, 1982, pp. 337–357. doi:10.1016/0022-460X(82)90244-9

[48] Mohseni, K., and Colonius, T., "Numerical Treatment of Polar Coordinate Singularities," *Journal of Computational Physics*, Vol. 157, No. 2, 2000, pp. 787–795. doi:10.1006/jcph.1999.6382

[49] Bogey, C., de Cacqueray, N., and Bailly, C., "Finite Differences for Coarse Azimuthal Discretization and for Reduction of Effective Resolution near Origin of Cylindrical Flow Equations," *Journal of Computational Physics*, Vol. 230, No. 4, 2011, pp. 1134–1146. doi:10.1016/j.jcp.2010.10.031

[50] Bogey, C., and Bailly, C., "Turbulence and Energy Budget in a Self-Preserving Round Jet: Direct Evaluation Using Large-Eddy Simulation," *Journal of Fluid Mechanics*, Vol. 627, 2009, pp. 129–160. doi:10.1017/S0022112009005801

[51] Bogey, C., and Bailly, C., "Three-Dimensional Non-Reflective Boundary Conditions for Acoustic Simulations: Far Field Formulation and Validation Test Cases," *Acta Acoustica*, Vol. 88, No. 4, 2002, pp. 463–471.

[52] Bogey, C., and Bailly, C., "Large Eddy Simulations of Transitional Round Jets: Influence of the Reynolds Number on Flow Development and Energy Dissipation," *Physics of Fluids*, Vol. 18, No. 6, 2006, p. 065101. doi:10.1063/1.2204060

[53] Hornung, H., and Schwendeman, D., "Oblique Shock Reflection from an Axis of Symmetry: Shock Dynamics and Relation to the Guderley Singularity," *Journal of Fluid Mechanics*, Vol. 438, 2001, pp. 231–245. doi:10.1017/S0022112001004360

[54] Troutt, T. R., and McLaughlin, D. K., "Experiments on the Flow and Acoustic Properties of Moderate-Reynolds-Number Supersonic Jet," *Journal of Fluid Mechanics*, Vol. 116, No. 1, 1982, pp. 123–156. doi:10.1017/S0022112082000408

[55] Norum, T. D., and Seiner, J. M., "Measurements of Mean Static Pressure and Far-Field Acoustics of Shock-Containing Supersonic Jets," NASA TM-84521, 1982.

[56] Freund, J. B., Lele, S. K., and Moin, P., "Compressible Effects in a Turbulent Annular Mixing Layer. Part 1. Turbulence and Growth Rate," *Journal of Fluid Mechanics*, Vol. 421, 2000, pp. 229–267. doi:10.1017/S0022112000001622

[57] Mohseni, K., Colonius, T., and Freund, J. B., "An Evaluation of Linear Instability Waves as Sources in a Supersonic Turbulent Jet," *Physics of Fluids*, Vol. 14, No. 10, 2002, pp. 3593–3600. doi:10.1063/1.1501545

[58] Ryu, J., Lele, S. K., and Viswanathan, K., "Investigation of Instability Waves in High-Speed Turbulent Jets," 13th AIAA/CEAS Aeroacoustics Conference, AIAA Paper 2007-3624, Rome, 2007.

[59] Tam, C. K. W., Chen, P., and Seiner, J. M., "Relationship Between Instability Waves and Noise of High-Speed Jets," *AIAA Journal*, Vol. 30, No. 7, 1992, pp. 1747–1752. doi:10.2514/3.11132

[60] Seiner, J., Bhat, T., and Ponton, M., "Mach Wave Emission from High-Temperature Supersonic Jet," *AIAA Journal*, Vol. 32, No. 12, 1994, pp. 2345–2350. doi:10.2514/3.12298

[61] Zaman, K. B. M. Q., "Effect of Initial Condition on Subsonic Jet Noise," *AIAA Journal*, Vol. 23, No. 9, 1985, pp. 1370–1373. doi:10.2514/3.9094

[62] Mclaughlin, D. K., Morrison, G. L., and Troutt, T. R., "Reynolds Number Dependence in Supersonic Jet Noise," *AIAA Journal*, Vol. 15, No. 4, 1977, pp. 526–532. doi:10.2514/3.60655

[63] Bodony, D. J., Ryu, J., and Lele, S. K., "Investigating Broadband Shock-Associated Noise of Axisymmetric Jets Using Large-Eddy Simulation," 12th AIAA/CEAS Aeroacoustics Conference, AIAA Paper 2006-2495, Cambridge, MA, 2006.

[64] Ponton, M. K., and Seiner, J. M., "The Effects of Nozzle Lip Thickness on Plume Resonance," *Journal of Sound and Vibration*, Vol. 154, No. 3, 1992, pp. 531–549. doi:10.1016/0022-460X(92)90784-U

[65] Petitjean, B. P., Viswanathan, K., and McLaughlin, D. K., "Acoustic Pressure Wave Forms Measured in High Speed Jet Noise Experiencing Nonlinear Propagation," *International Journal of Aeroacoustics*, Vol. 5, No. 2, 2006, pp. 193–215. doi:10.1260/147547206777629835

[66] Gee, K. L., Sparrow, V. W., James, M. M., Downing, J. M., Hobbs, C. M., Gabrielson, T. B., and Atchley, A. A., "The Role of Nonlinear Effects in the Propagation of Noise from High-Power Aircraft," *Journal of the Acoustical Society of America*, Vol. 123, No. 6, 2008, pp. 4082–4093. doi:10.1121/1.2903871

[67] Norum, T. D., "Screech Suppression in Supersonic Jets," *AIAA Journal*, Vol. 21, No. 2, 1983, pp. 235–240. doi:10.2514/3.8059

P. Tucker
Associate Editor